International Journal of Steel Structures (2019) 19(1):241–254
https://doi.org/10.1007/s13296-018-0113-z

Online ISSN 2093-6311
Print ISSN 1598-2351

Dynamic Crushing Behaviors of Aluminum Foam Filled Energy Absorption Connectors

Yonghui Wang[1,2] · **Ximei Zhai**[1,2]

Received: 6 March 2018 / Accepted: 20 June 2018 / Published online: 22 June 2018

Abstract

This paper presented the numerical studies on the dynamic crushing behaviors of the aluminum foam filled energy absorption connectors. The finite element (FE) model was firstly constructed and the accuracy of the FE model was verified by comparing the force–displacement curves from FE analyses with those from tests and analytical predictions. The numerical results revealed that the deformation mode of the connector under dynamic crushing evidently differed from that under quasi-static loading mainly due to the inertia effect. Besides, the energy absorption capacity was also improved when the dynamic crushing load was applied. Then, the parametric studies on the effects of crushing velocity–time history, angle between flat plate and pleated plate as well as pleated plate thickness on the energy absorption enhancements of the connectors were conducted. Based on the numerical results, two empirical equations were derived in terms of various parameters to predict the energy absorption enhancements of aluminum foam and pleated plate, which could be employed to obtain the force–displacement functions of the connectors under dynamic crushing.

Keywords Aluminum foam · Deformation mode · Dynamic crushing · Energy absorption connector · Numerical study

1 Introduction

The probability of blast attack on buildings has shown an increasing tread in recent years and therefore many blast resistant façades/panels were developed in order to reduce the blast-induced damage on the buildings (Wang et al. 2015, 2016; Ngo et al. 2015; Zhang et al. 2015; Huang et al. 2015; Huang and Liew 2016; Zhu and Khanna 2016). The blast load transferred to the building may be considerably high if the 'rigid' connection between the façade/panel and building is adopted, which may lead to severe damage of the building. Therefore, the 'soft' connection between the façade/panel and building via energy absorption connectors was recently developed (Amadio and Bedon 2012a, b; Wang et al. 2017c), which showed better performance than the 'rigid' connection in terms of dissipating part of blast energy and reducing peak blast load transferred to the building (Amadio and Bedon 2014; Wang and Liew 2015). Up to date, several types of energy absorption connectors made of metallic material were developed to resist relatively low blast pressure (Hallissy et al. 2005; Whitney 1996). Such energy absorption connectors relied on plastic deformation of pleated plate to absorb blast energy. Besides this, Amadio and Bedon (2012a) developed a dissipative device for the blast mitigation of glazing façade supported by prestressed cables, which was shown to mitigate the severe structural damage of critical components of the façade as well as to dissipate part of the blast-induced stresses in the critical façade components (Amadio and Bedon 2014). As for the case with relatively high blast load, the connector with higher energy absorption capacity was necessary, which promoted the development of aluminum foam filled energy absorption connectors shown in Fig. 1. The connector was designed with mild steel as face plates and aluminum foam as core energy absorption material. Hence, both plastic deformation of pleated plate and compression of aluminum foam contributed to the energy absorption. The energy absorption performance of the connector under quasi-static

✉ Yonghui Wang
wangyonghui@hit.edu.cn

1 Key Lab of Structures Dynamic Behavior and Control of the Ministry of Education, Harbin Institute of Technology, Harbin 150090, China

2 Key Lab of Smart Prevention and Mitigation of Civil Engineering Disasters of the Ministry of Industry and Information Technology, Harbin Institute of Technology, Harbin 150090, China

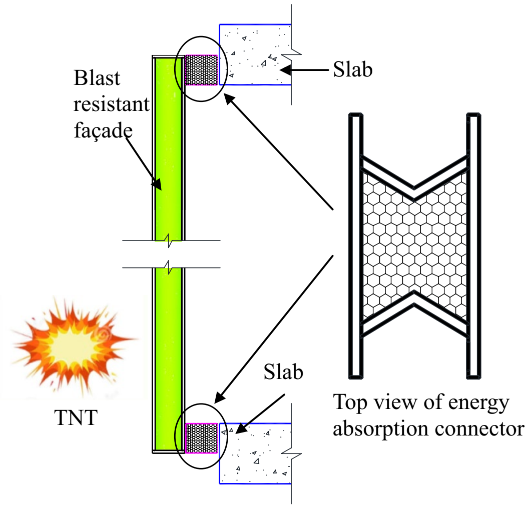

Fig. 1 Application of energy absorption connector

crushing load was experimentally, numerically and analytically studied by the authors (Wang et al. 2017a, b) and it was found that the filled aluminum foam could considerably improve the energy absorption capacity of the connector (Wang et al. 2017b). Since the connector experienced dynamic crushing under blast load and its deformation mode and energy absorption performance might show some differences as compared to those under quasi-static crushing (Baroutaji et al. 2016; Fan et al. 2013). Hence, the aim of this work is to study the behaviors of the proposed energy absorption connectors under dynamic crushing and develop the empirical equations to predict the energy absorption enhancements.

In the past, metallic material was usually adopted as energy absorbers which were designed to dissipate energy via plastic deformation (Baroutaji et al. 2014; Baroutaji et al. 2015a; Gupta et al. 2005; Wang 1987; McDevitt and Simmonds 2003; Niknejad and Orojloo 2016; Fan et al. 2015), splitting of steel plate and friction (Chen et al. 2016) as well as free inversion of circular tubes (Zhang et al. 2009). Besides the studies on the metallic energy absorbers under quasi-static loading, its behaviors under dynamic loading were also investigated (Su et al. 1995a; b; Baroutaji et al. 2016; Olabi et al. 2008a; b) and the observed different energy absorption behaviors could be attributed to the inertia and strain rate effect (Su et al. 1995a; b).

Recently, metal foams have been increasingly used to absorb blast and impact energy due to the lightweight and high energy absorption capacity, and the improvement in energy absorption capacity was evident when filling the tubes with metal foams (Reyes et al. 2004a; Hall et al. 2002; Shen et al. 2015). The crushing behaviors and energy absorption performances of the energy absorbers under quasi-static loading were extensively studied (Santosa et al. 2000; Reyes et al. 2004a; Hall et al. 2002; Shen et al. 2015; Baroutaji et al. 2015b; Reyes et al. 2004b). For the metal foam-filled square columns under axial compression loading, the increase of mean crushing force was found to be linearly dependent on the foam compression resistance and cross-sectional area of the column (Santosa et al. 2000). The energy absorption performances of the metal foam-filled square columns under oblique loading were also experimentally and numerically studied and it was found that the high-density aluminum foam filler could increase the energy absorption capacity but showed some reduction in specific energy absorption as compared to the empty cross sections (Reyes et al. 2004a). As for the metal foam-filled tubes under lateral compression loading (Hall et al. 2002; Shen et al. 2015; Baroutaji et al. 2015b), it showed fewer fluctuations in load and low amplitude of peak load, which were more desirable as an energy absorber (Shen et al. 2015). Since the energy absorbers usually experienced dynamic crushing load, their dynamic crushing behaviors were also extensively studied (Shahbeyk et al. 2007; Smith et al. 2016; Fan et al. 2013; Yang and Qi 2013). The multiobjective optimization of foam-filled square columns under oblique impact loading was conducted by Yang and Qi to maximize the specific energy absorption and minimize the peak crushing force and it was found that the optimal designs were generally different with varying load angles (Shahbeyk et al. 2007). As for the aluminum foam filled braided stainless steel tubes subjected to transverse impact loading, it was found that aluminum foam cores possessing a density level exceeding 400 kg/m^3 might mitigate the desired foam crushing effect due to incompatibilities between the mechanical strengths of the aluminum foam core and braided tube (Smith et al. 2016). The dynamic lateral crushing behaviors of sandwich circular tubes, which consisted of two concentric aluminum tubes of different diameters filled with aluminum foam, were also examined by Fan et al. (2013). It was found that significant increase was shown for the dynamic crushing load. Moreover, the energy absorption over its quasi-static counterpart and the deformation profile also showed some differences, which could be attributed to the inertia effect under dynamic crushing.

In the present study, the explicit code in LS-DYNA, which was widely used to simulate the crushing behavior of aluminum foam (Reyes et al. 2003; Hanssen et al. 2002; Qi et al. 2013; Shim et al. 2013), was utilized to analyze the deformation mode and energy absorption enhancements of the aluminum foam filled connectors under dynamic crushing. The accuracies of the FE models were verified against test results and analytical predictions. Then, the deformation mode and energy absorption of the connector under quasi-static and dynamic crushing were compared. In addition, the parameters that affected the energy absorption enhancements of the connectors under dynamic crushing were discussed and two empirical equations for determining the energy absorption enhancements of aluminum foam and pleated plate were also presented.

2 FE Model Establishment and Verification

The quasi-static compression loading tests on the proposed aluminum foam filled energy absorption connectors were conducted by the authors (Wang et al. 2017a). The specimens, test setup and instrumentation were summarized in this section and the test results and analytical predictions were adopted herein to validate the FE models described in this section.

2.1 Summary of Tests on Energy Absorption Connectors

2.1.1 Specimens

The aluminum foam filled energy absorption connectors were fabricated from mild steel as face plates and closed cell aluminum foam as core energy absorption material. The closed cell aluminum foam generally shows three deformation stages under uniaxial compression loading, i.e., initial elastic deformation, plastic deformation and densification stage. The strain within plastic deformation stage is considerably higher as compared to the other two deformation stages and the stress in this stage also shows nearly constant, both of which are desirable for the energy absorption material. As shown in Fig. 2, the pleated plates were bolted to the top and bottom plate to form a closed space where the aluminum foam was inserted thereafter. The reentrant pleated plates instead of salient pleated plate or flat plate was adopted, since it could provide confinement on the aluminum foam and showed fixed plastic hinges during crushing. The selected connectors for the FE model verification are summarized in Table 1 and the varying parameters include pleated plate thickness and angle θ_o (the angle between flat plate and pleated plate). The material properties of mild steel and aluminum foam in Table 2 are obtained from the tensile coupon test and uniaxial compression loading test, respectively. The geometry of the test specimens are illustrated in Fig. 2 and summarized in Table 1.

2.1.2 Test Setup and Instrumentation

A material testing machine (MTS) of 1000 kN capacity was employed to apply the quasi-static compression load on the connectors. As shown in Fig. 3 for the test setup and instrumentation, the connector was inserted between the actuator and I beam support and the load was applied through moving down the actuator. In order to ensure a quasi-static loading rate, the actuator moved downwards at a speed of 0.5 mm/min before yield and the speed was gradually increased to 2 mm/min thereafter. Two 20 mm thick steel plates were bolted to the connector on the top and bottom plate, respectively, to avoid the bending of these two flat plates as well as to be consistent with the actual boundary condition shown in Fig. 1. Two Linear Variable Displacement Transducers (LVDTs) were employed to measure the displacement of the connector and a load cell was installed on the actuator to measure the compressive force. The readings of LVDTs and load cell were recorded using a data logger. The force–displacement curves of the connectors obtained in this test would be used to verify the FE model in the following section.

2.2 FE Modeling of Energy Absorption Connector

2.2.1 Material Models

The Piecewise Linear Plasticity material model (Hallquist 2006) in LS-DYNA was employed to simulate the mild steel. The input true stress–effective plastic strain curves of the mild steels used in the connectors were obtained from the tensile coupon tests. The material properties of mild steels with variant thicknesses are given in Table 2 and the input true stress–effective plastic strain curves are shown in Fig. 4a. In this material model, the Cowper-Symonds model is adopted to scale the yield stress as

$$\sigma_y\left(\varepsilon_{eff}^p, \dot{\varepsilon}_{eff}^p\right) = \sigma_y\left(\varepsilon_{eff}^p\right)\left[1 + \left(\frac{\dot{\varepsilon}_{eff}^p}{C}\right)^{1/P}\right] \quad (1)$$

where $\sigma_y(\varepsilon_{eff}^p)$ is the yielding stress without considering strain rate effects, $\dot{\varepsilon}_{eff}^p$ is the effective plastic strain rate, C and P are the strain rate parameters. In this study, the strain rate parameters C and P are 40.4 s^{-1} and 5 for mild steel (Jones 1988). Since there was no failure of mild steel being observed in the test, the failure criteria specified in this material model in the form of effective plastic strain and element eroding was not defined.

Several material models are available in LS-DYNA to simulate the crushing behavior of aluminum foam, e.g., MAT 26, 63, 75, 126 and 154. Hanssen et al. (2002) noted that MAT 63 and 75 showed the best performance and highest computational efficiency by comparing the experimental results with numerical predictions utilizing these material models. In the present work, the MAT 63, i.e., crush foam with optional damping and tension cutoff, was adopted to simulate the mechanical behavior of aluminum foam. The yield of MAT 63 is governed by the largest principle stress, i.e., the principle stresses σ_1, σ_2 and σ_3 are compared with

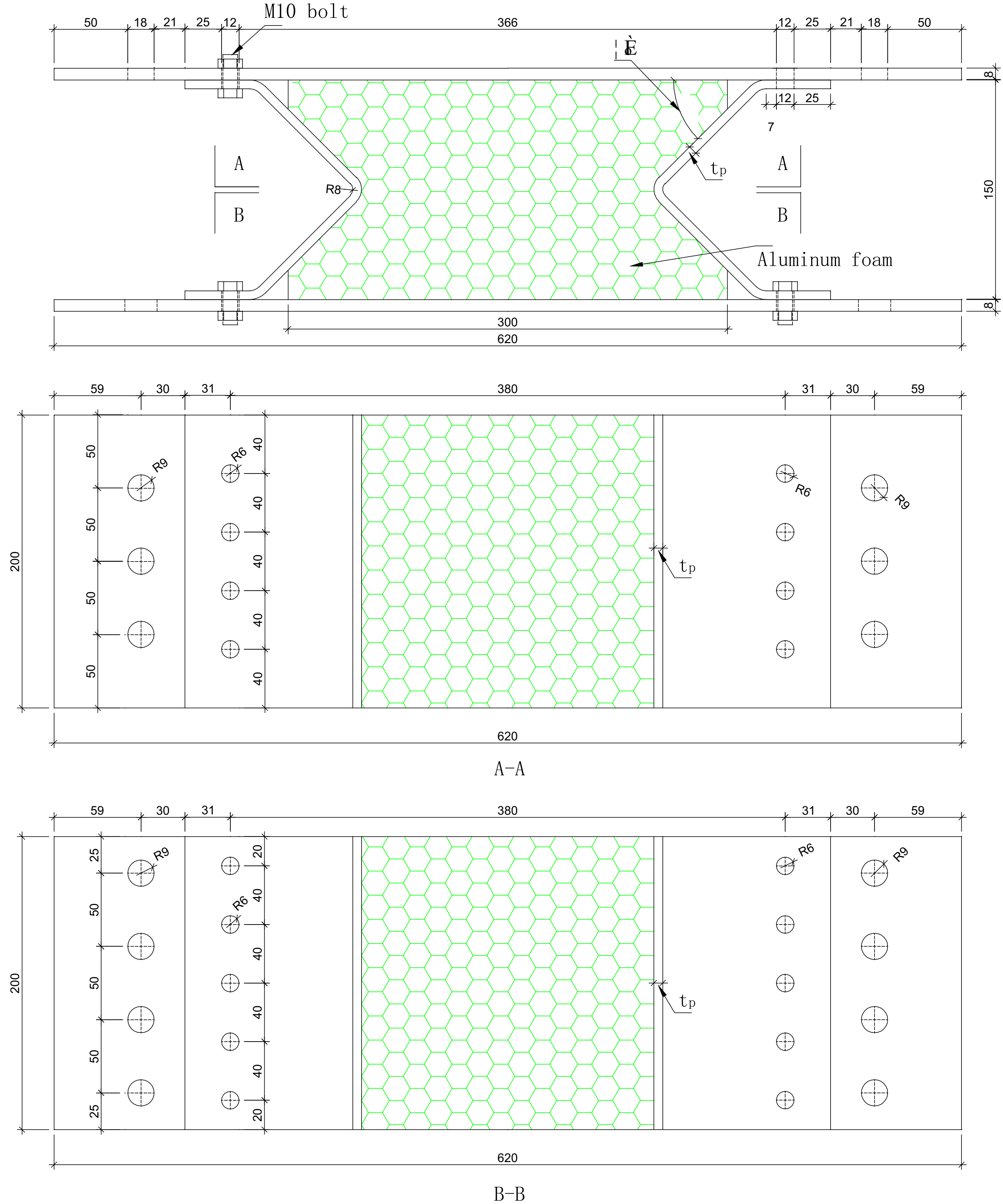

Fig. 2 Dimensions of energy absorption connector (in mm)

Table 1 Geometry of the energy absorption connectors

Specimen	θ_o (°)	t_p (mm)
Pt4	45	4
Pc	45	6
Pt8	45	8
Pa30	30	6
Pa60	60	6

θ_o, angle between flat plate and pleated plate; $t_{p,}$ Pleated plate thickness

Table 2 Material properties of mild steel and aluminum foam

Mild steel	E_y (GPa)	σ_y (MPa)	σ_u (MPa)
$t_p=4$ mm	202.8	300.9	429.9
$t_p=6$ mm	204.6	298.2	445.9
$t_p=8$ mm	217.7	363.9	485.0
Aluminum foam	ρ_f (g/cm^3)	σ_P (MPa)	E_f (MPa)
–	0.305	1.8	95.4

E_y, E_f, Young's modulus of steel and aluminum foam; σ_y, yield stress of steel; σ_u, ultimate stress of steel; ρ_f, density of aluminum foam; σ_P, Plateau stress of aluminum foam

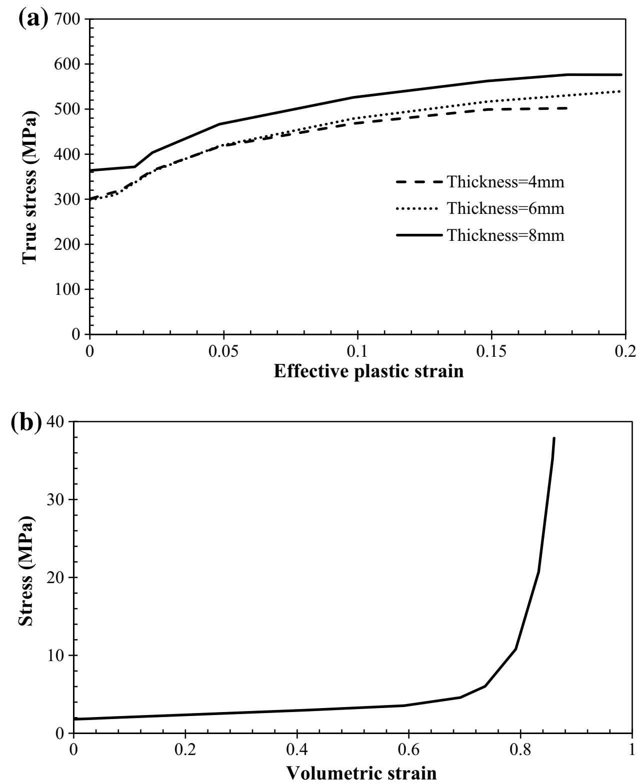

Fig. 4 Input stress–strain curves in FE model: **a** true stress–effective plastic strain curves for mild steels and **b** stress–volumetric strain curve for aluminum foam

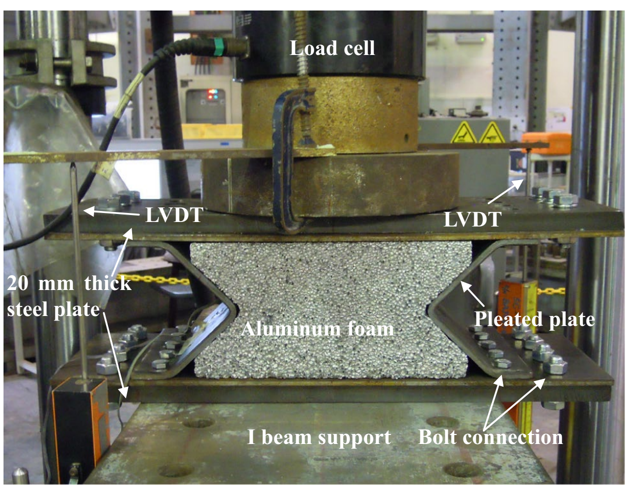

Fig. 3 Test setup and instrumentation

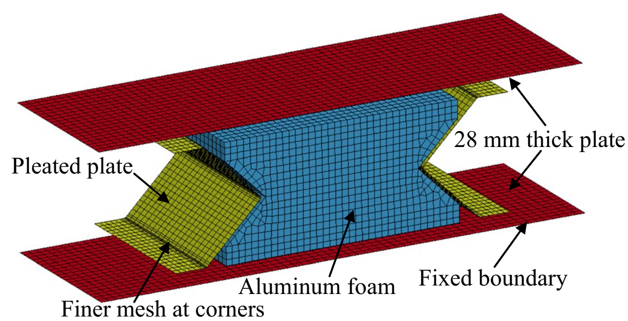

Fig. 5 FE model of energy absorption connector

the yield stress Y and Y_t for compressive and tensile principle stress component, respectively. Y is a yield stress from a user-defined volumetric strain-hardening function and Y_t is a constant tensile cutoff stress (Hanssen et al. 2002). Table 2 gives the material properties of aluminum foam, which were obtained from uniaxial compression loading tests. Figure 4b shows the input yield stress Y versus volumetric strain curve. The plastic Poisson's ratio is set to a small value (0.01), since the aluminum foam nearly shows no lateral expansion under uniaxial compression loading (Yang and Qi 2013).

2.2.2 Model Description

Figure 5 shows the FE model of the energy absorption connector. The mild steel plates of the connector were meshed using S/R Hughes-Liu shell element with five integration points along the thickness and eight-node solid element with reduced integration in combination with hourglass control was employed for the aluminum foam. The element sizes of the pleated plate and aluminum foam were 7 and 8.5 mm, respectively. Finer mesh with element size of 1 mm perpendicular to the width direction was applied at the corners of pleated plate to capture the smooth curvature change and severe local deformation. The penalty-based contact approach in LS-DYNA, which is suitable for modeling contact between bodies of similar materials, was adopted for the contact between steel plates. The soft constraint-based contact approach, which is suitable for treating contact between bodies of dissimilar materials, was employed for the contact between steel plates and aluminum foam. As shown in Fig. 3, the 8 and 20 mm steel plates were bolted together in the test and no separation was observed during the compression loading test. Hence, the single steel plate with 28 mm thickness was chosen as an alternative, as shown in Fig. 5. The fixed boundary condition was applied to the steel plate at the bottom by restricting all the nodes on the bottom plate from translation and rotation. The top steel plate was specified with a linearly varying downward velocity to apply the dynamic crushing load. The perfect bolt connection was applied in the FE model by connecting the selected nodes on pleated plates to flat plates through *CONTACT_TIED_SHELL_EDGE_TO_SURFACE in LS-DYNA (Hallquist 2012).

2.3 FE Model Verification

In order to verify the established FE models with the test results and analytical predictions, the top steel plate was specified with a low constant downward velocity and the kinetic energy was kept to be less than 5% of internal energy to ensure a quasi-static loading rate. The collapse process of the connector Pc from FE simulations is compared with the test observations in Fig. 6. As for the pleated plate, the curvature change of pleated plate at plastic hinge locations (mid-height and near the bolts) and along the pleated plate can be clearly seen from the FE simulations, which is in agreement with the test observations. As for the crushing of aluminum foam, cracking and following separation is observed at the front and rear surfaces of the aluminum foam under severe compression due to the absence of lateral confinement on the two surfaces. However, the separation portion of aluminum foam is not significant. This is not captured in the FE simulations, since the failure of aluminum foam, which shows negligible effect on the FE results, is not defined in the FE model. Figure 7a compares the compressive force–displacement curves of the energy absorption connectors obtained from tests and FE predictions and good match between the two can be observed in the elastic and plastic deformation stage. However, the FE predictions show slight delay in entering aluminum foam densification stage, in which the aluminum foam reaches densification and the compressive force shows sudden increase. The possible reason is that the density of aluminum foam in the test is not uniformly distributed, which is difficult to capture in the FE model. A better agreement between the FE and analytical predictions can be observed in Fig. 7b, which shows reasonable match of the compressive force–displacement curves in both plastic deformation and aluminum foam densification stage due to the assumed uniformly distributed density of aluminum foam in these two models. Based on above comparisons, the established FE models are proven to be reasonable and can be used to study the response behaviors of the aluminum foam filled energy absorption connectors under dynamic crushing.

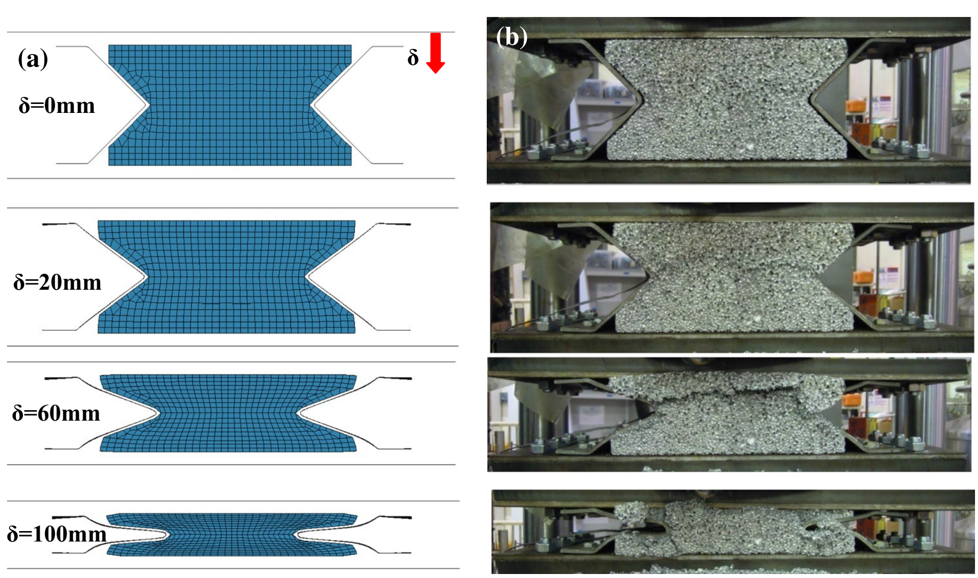

Fig. 6 Comparison of collapse process of connector Pc: **a** FE results and **b** test results

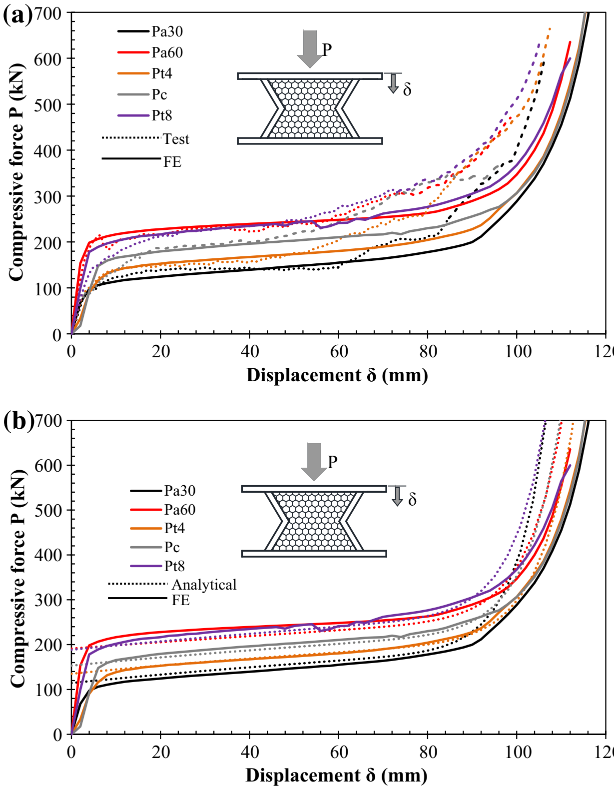

Fig. 7 Comparison of force–displacement curves: **a** test versus FE predictions and **b** analytical versus FE predictions

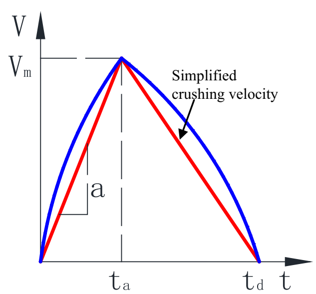

Fig. 8 Simplification of crushing velocity–time history of connector

3 Dynamic Crushing Behavior

3.1 Crushing Velocity–Time History

Since the aluminum foam filled energy absorption connector is proposed to be inserted between a façade and a building, it will immediately start to crush after exposed to blast load and the crushing velocity of the connector (in Fig. 8) continuously rises to the peak value and thereafter drops to zero. Meanwhile, the connector reaches the ultimate crushing stage. Due to coupling effects between the blast resistant façade/panel and connector, the crushing velocity–time history profile varies with the blast load history and mechanical properties of blast resistant façade/panel and connector. In order to study the dynamic crushing behaviors of the connector and develop the formulas to predict the energy absorption enhancements in terms of the parameters of crushing velocity–time history, a fixed crushing velocity–time history profile is necessary. Hence, a simplified crushing velocity with linear variation was adopted in this study, which is close to the actual crushing velocity–time history (i.e., the crushing velocity shows monotonic increase to the peak value and then monotonically drops to zero). V_m, a, t_a and t_d in Fig. 8 stand for peak crushing velocity, positive acceleration, positive acceleration duration and total crushing duration, respectively. In the following calculations, a and t_a can be chosen as varying parameters and V_m is determined once a and t_a are determined. The value of t_d is determined by ensuring that the total crushing displacement, S_c, of the connector is constant (i.e., $S_c = \int_0^{t_d} Vdt = const.$) and slightly larger than the densification displacement of the connector. The densification displacement is the crushing displacement when the aluminum foam reaches densification and the compressive force shows sudden increase. Herein, S_c is determined as 125 mm, which is larger than the densification displacements of the connectors, as shown in Fig. 7. In order to reveal the different behaviors of the connector under quasi-static and dynamic crushing, the connector Pc was applied with the quasi-static and dynamic crushing loads by specifying the top steel plate with different velocity–time histories. To apply the dynamic crushing load, the linearly varying velocity–time history with $a = 7.46E6$ m/s^2 and $t_a = 0.0134$ ms was applied, which was corresponding to $V_m = 100$ m/s.

3.2 Deformation Modes and Energy Dissipation

Figure 9 compares the deformation modes of the connector Pc under quasi-static and dynamic crushing loads and the differences of the deformation modes of aluminum foam are evident, i.e., the uniform crushing of aluminum foam is observed under quasi-static crushing load and the non-uniform crushing of aluminum foam with crushing initiating at the top is observed under dynamic crushing load. This phenomenon can also be proven by comparing the compressive strains of aluminum foam at upper and lower layer under quasi-static and dynamic crushing loads in Fig. 10. The compressive strains of aluminum foam at upper and lower layer are almost same under quasi-static crushing. As for the connector under dynamic crushing, the compressive strain at upper layer shows rapid increase at initial crushing stage and thereafter remains a constant value when the aluminum foam at upper layer reaches densification. Meanwhile, the aluminum foam at lower layer shows delay in developing compressive strain and the value

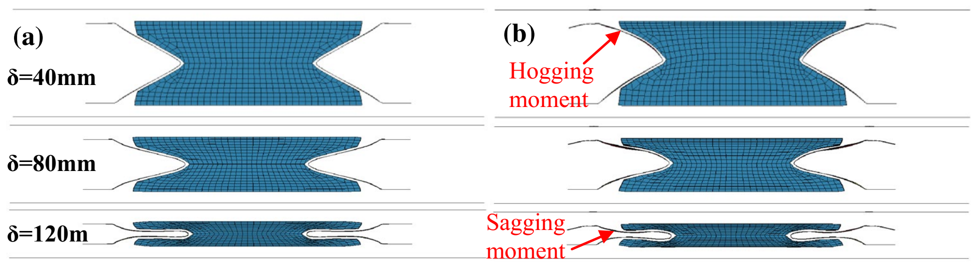

Fig. 9 Deformation modes of the connecter under **a** quasi-static and **b** dynamic crushing

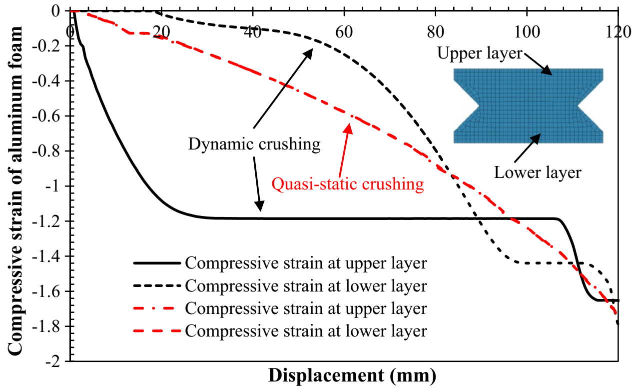

Fig. 10 Compressive strain of aluminum foam at upper and lower layer

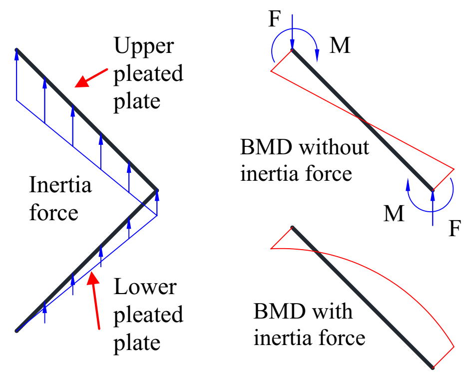

Fig. 12 Effect of inertia force on the bending moment diagram (BMD) of upper pleated plate

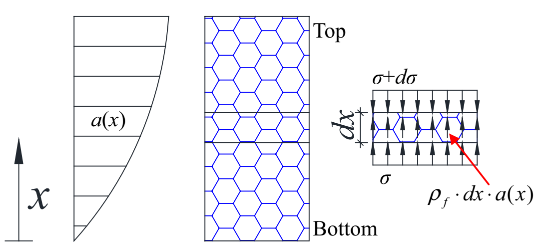

Fig. 11 Effect of inertia force on the stress distribution along the aluminum foam depth

is also lower as compared to upper layer. However, the compressive strains of aluminum foam at upper and lower layer approach each other with relatively larger deformation when the aluminum foam at lower layer also reaches densification. At this moment, the compressive strains of aluminum foam are almost uniformly distributed under both quasi-static and dynamic crushing loads.

The non-uniform crushing of aluminum foam under dynamic crushing is mainly due to the inertia effect. As illustrated in Fig. 11, due to the existing of inertia force under dynamic crushing, the compressive stress variation along the depth of aluminum foam, $d\sigma$, can be determined as

$$d\sigma = \rho_f a(x)dx \tag{2}$$

where ρ_f is aluminum foam density and $a(x)$ is acceleration. Hence, the compressive stress of aluminum foam shows highest value at the top and lowest value at the bottom. This leads to the crushing of aluminum foam initiating at the top.

The deformation mode of pleated plates also shows some differences under dynamic crushing. As shown in Fig. 9, the upper and lower pleated plates show symmetric deformation mode when the quasi-static crushing load is applied. As for the connector under dynamic crushing, the upper pleated plate develops evident hogging moment at initial crushing stage and finally changes to sagging moment, while the deformation mode of lower pleated plate is similar to the case under quasi-static crushing. The change of deformation mode of the upper pleated plate under dynamic crushing is also due to the inertia effect. As illustrated in Fig. 12, the acceleration along the pleated plate is almost linearly distributed at initial crushing stage before the evident change of deformation mode and it is same with the inertia force distribution. Hence, the upper pleated plate with higher acceleration and inertia force is easier to behave deformation mode changing. Figure 12 shows the bending moment diagram (BMD) of upper pleated plate with inertia force considered, which can explain the hogging moment of upper pleated plate at initial crushing stage observed in Fig. 9b.

Figure 13 compares the energy absorption–displacement curves of the connector Pc under quasi-static and dynamic crushing loads and the significant increase in energy

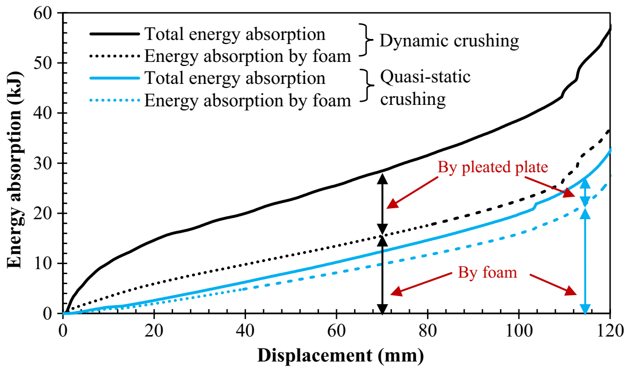

Fig. 13 Energy absorption–displacement curves of the connecter under dynamic and quasi-static crushing

absorption under dynamic crushing is observed. It is also noted that the pleated plate contributes more to the energy absorption improvement due to the change of deformation mode and strain rate effect. Taking the energy absorption of the connector Pc at 100 mm displacement for instance, the total energy absorption under dynamic crushing is increased by 94.1% as compared to that under quasi-static crushing. As for the energy absorption increase of each component, 40.9 and 312.9% increases of energy absorption are observed for aluminum foam and pleated plate, respectively.

Figure 14 compares the energy absorption–displacement curves of upper and lower pleated plates under quasi-static and dynamic crushing loads. It is noted that the upper pleated plate dissipates more energy as compared to the lower pleated plate under dynamic crushing. This can be attributed to higher strain rate at the upper pleated plate and more significant plastic strain energy accumulation by the change of hogging moment to sagging moment during dynamic crushing. In terms of the connecter under quasi-static crushing, the upper and lower pleated plate dissipates comparable energy. Although the deformation mode of lower pleated plate under dynamic crushing is similar to that under quasi-static crushing, improved energy absorption is observed for the lower pleated plate under dynamic crushing with displacement lager than 40 mm, which can be attributed to the enhanced yield strength of pleated plate induced by strain rate effect.

The resultant force–displacement curves of the connecter at upper and lower layers under quasi-static and dynamic crushing loads are compared in Fig. 15. When the dynamic crushing load is applied, the resultant force at upper layer initially shows significantly higher value than that at lower layer due to the aforementioned inertia effect. However, the resultant forces at upper and lower layers approach to each other thereafter with the continuous crushing of the connector, which are also close to the resultant forces of the connector under quasi-static crushing.

4 Energy Absorption Enhancement Under Dynamic Crushing

The analytical force–displacement function of the proposed energy absorption connecter under quasi-static crushing was presented by Wang et al. (2017a). Since the connector experiences a dynamic crushing load in the event of blast attack, the dynamic crushing induced force–displacement function of the connector is necessary to more accurately represent the energy absorption capacity of the connector. Herein, the energy absorption enhancement (the dynamic energy enhancement over its static one) of the connector, together with the analytical force–displacement function proposed by Wang et al. (2017a), are used to yield the dynamic crushing induced force–displacement function of the connector, which can be approximately determined by scaling up the force–displacement function of the quasi-static loaded connector with the energy absorption enhancement. It is noted in Fig. 16 that the energy absorption enhancement shows significant decrease at initial crushing stage and approaches

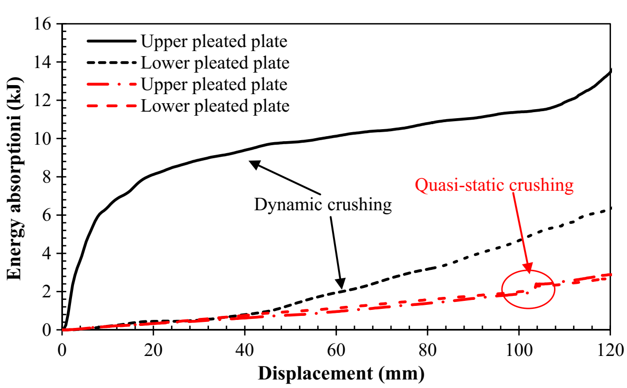

Fig. 14 Energy absorption–displacement curves of pleated plates under dynamic and quasi-static crushing

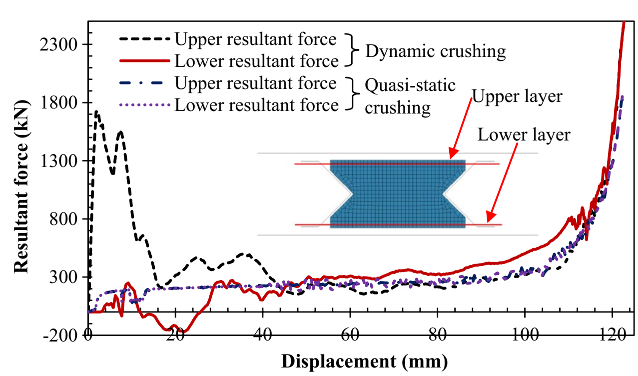

Fig. 15 Resultant force–displacement curves of the connector under dynamic and quasi-static crushing

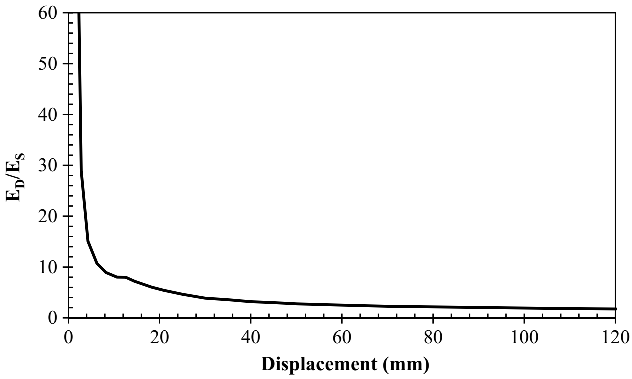

Fig. 16 Energy absorption enhancement versus displacement

a stable value with relatively larger deformation. In the blast resistant design, it is preferred to make full use of the connector to dissipate blast energy. Hence, the adopted energy absorption enhancement in the following discussions is corresponding to the displacement when the connector reaches the ultimate energy absorption capacity and the compressive force shows sudden increase (shown in Fig. 15). This energy absorption enhancement is also conservative for the case when the connector does not reach the ultimate energy absorption capacity. Herein, the energy absorption enhancement at 100 mm displacement was adopted.

The parametric studies on the effects of crushing velocity–time history (a and t_a), angle θ_o, pleated plate thickness on the energy absorption enhancement are presented in this section and two empirical equations are derived in terms of various parameters to predict the energy absorption enhancements of aluminum foam and pleated plate.

4.1 Effect of *a* and t_a

As previous observations, the different responses of the connector under quasi-static and dynamic crushing loads were mainly due to the inertia effect. Hence, positive acceleration, a, and positive acceleration duration, t_a, of the crushing velocity–time history were adopted as the varying parameters.

Since positive acceleration, a, and positive acceleration duration, t_a, determine the magnitude and duration of inertia force, respectively, the energy absorption enhancement of the connector is thought to be closely related to a and t_a. Figure 17 shows the effects of a and t_a on the energy absorption enhancements of aluminum foam and pleated plate, and increasing either a or t_a can lead to an increase in energy absorption enhancement. The energy absorption enhancement of pleated plate with relatively higher a and t_a is evidently higher than that of aluminum foam.

In order to combine the effects of a and t_a on the energy absorption enhancement, the peak crushing velocity, V_m,

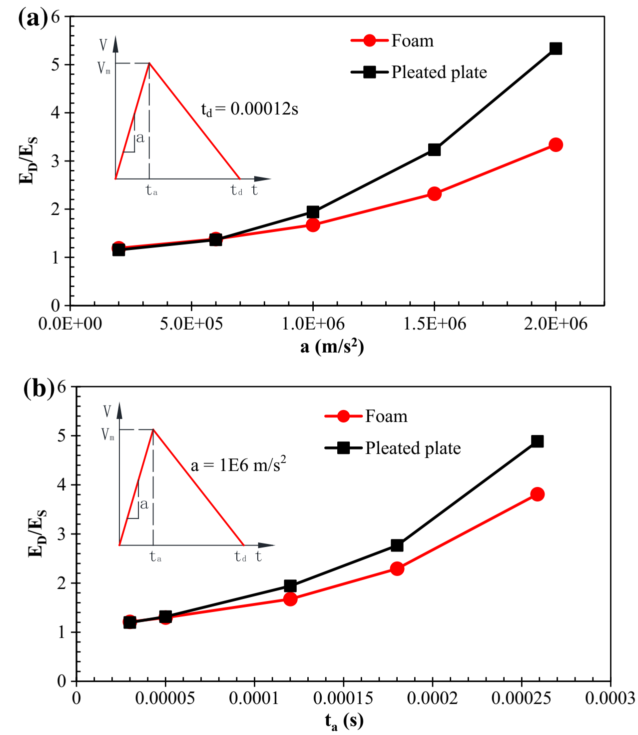

Fig. 17 Effect of **a** a and **b** t_a on the energy absorption enhancement

which can be determined by multiplying a by t_a, is adopted and Fig. 18 plots the energy absorption enhancements of aluminum foam and pleated plate versus V_m. It is noted that the energy absorption enhancement of aluminum foam seems to be only related to V_m. As for the pleated plate, the energy absorption enhancement versus V_m curve obtained by varying a evidently differs from that obtained by varying t_a when V_m is higher than 120 m/s. Hence, in the following discussions, the energy absorption enhancement of aluminum foam is only plotted with respect to V_m and the energy absorption enhancement of pleated plate is plotted with respect to a and t_a.

4.2 Effect of Angle θ_o

Figure 19 shows the effect of angle θ_o on the energy absorption enhancement of aluminum foam. It is noted that angle θ_o rarely affects the energy absorption enhancement when peak crushing velocity, V_m, is less than 72 m/s, which could be attributed to the insignificant inertia effect with relatively small value of V_m. However, decreasing angle θ_o leads to an increase in energy absorption enhancement with higher V_m and the increase magnitude of energy absorption enhancement is more significant with increasing V_m. The effect of angle θ_o on the energy absorption enhancement of pleated plate is given in Fig. 20, which shows that increasing angle θ_o leads to an significant decrease in energy absorption

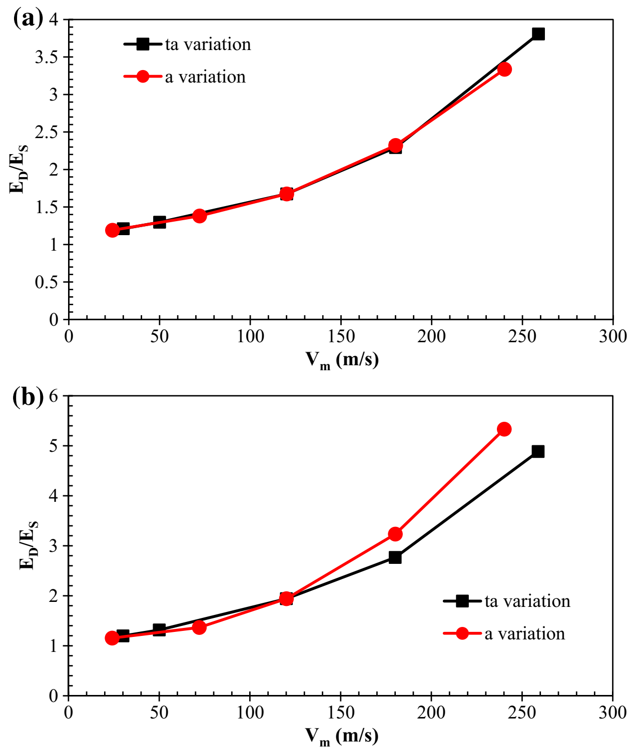

Fig. 18 Effect of V_m on the energy absorption enhancement: **a** aluminum foam and **b** Pleated plate

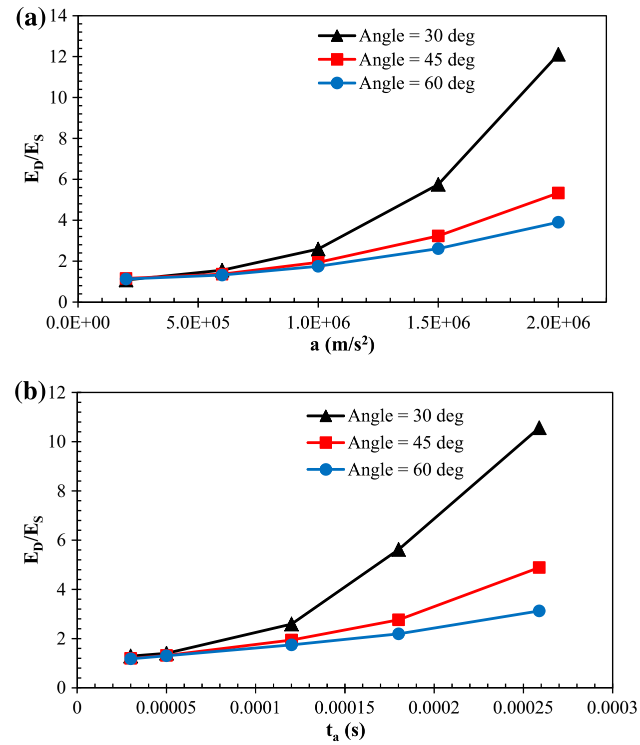

Fig. 20 Effect of angle θ_o on the energy absorption enhancement of pleated plate versus **a** a and **b** t_a

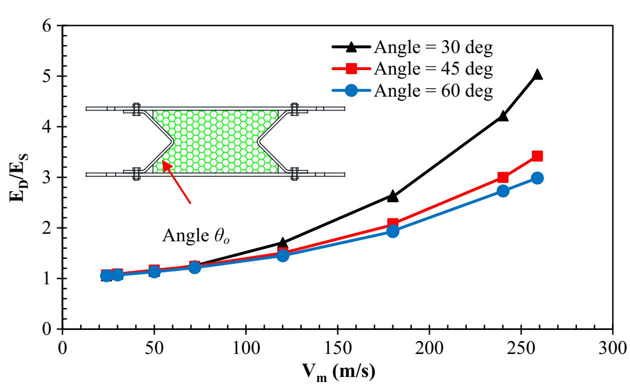

Fig. 19 Effect of angle θ_o on the energy absorption enhancement of aluminum foam versus V_m

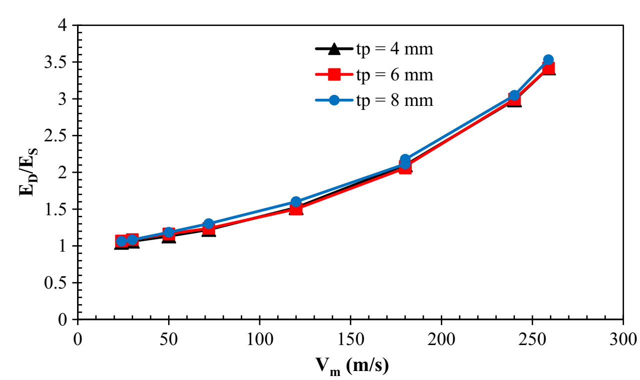

Fig. 21 Effect of pleated plate thickness on the energy absorption enhancement of aluminum foam versus V_m

enhancement of pleated plate, especially with higher a and t_a. The pleated plate mainly relies on plastic hinge rotation at corners to absorb energy under quasi-static crushing. As for the connector under dynamic crushing, besides the energy absorption contribution from plastic hinge rotation, the flat part of upper pleated plate also contributes to the energy absorption by the change of hogging moment to sagging moment induced by inertia effect, as illustrated in Fig. 12. The connector with smaller angle θ_o has longer upper pleated plate, which leads to the higher energy absorption contributed by the upper pleated plate under dynamic crushing as well as the higher energy absorption enhancement.

4.3 Effect of Pleated Plate Thickness

Figure 21 shows the effect of pleated plate thickness on the energy absorption enhancement of aluminum foam which is found to be rarely affected by the variation of pleated plate thickness. This is because the variation of pleated plate thickness nearly has no effect on the volume and deformation mode of aluminum foam, both of which determine the energy absorption of aluminum foam. The effect of pleated plate thickness on the energy absorption enhancement of pleated plate is compared in Fig. 22. It is noted that decreasing pleated plate thickness leads to an increase in energy absorption enhancement of pleated plate, especially with higher a and t_a. Since the energy absorption improvement of pleated plate under dynamic crushing is due to the strain rate effect and deformation mode change, the thinner pleated plate may behave more significant deformation mode change, which leads to more significant increase of energy absorption with thinner pleated plate.

4.4 Empirical Equations for Determining the Energy Absorption Enhancement

The previous parametric studies revealed the significance of parameters that affect the energy absorption enhancements of aluminum foam and pleated plate. It was noted that the energy absorption enhancement of aluminum foam was strongly dependent on V_m and angle θ_o. Hence, an empirical equation was derived through multivariable regression analysis in terms of two non-dimensional parameters to predict the energy absorption enhancement of aluminum foam, EAE_f, as shown in Eq. (3).

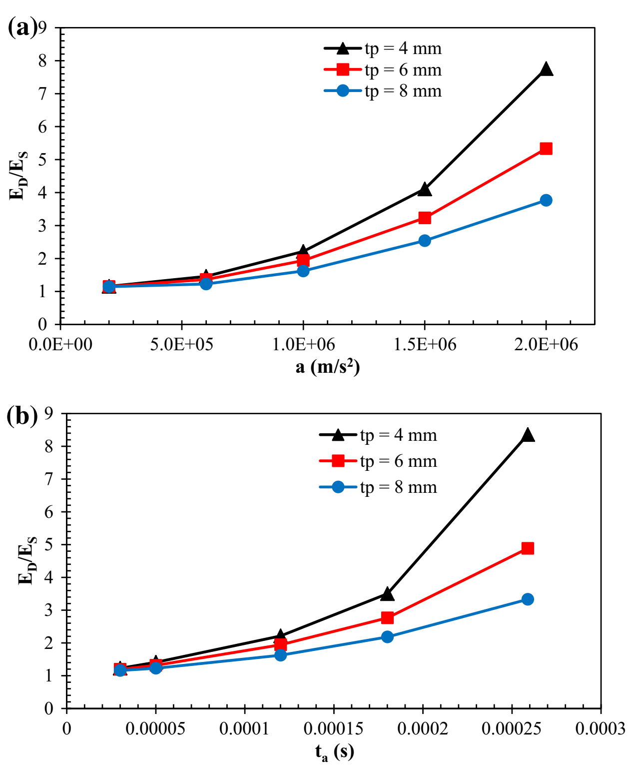

Fig. 22 Effect of pleated plate thickness on the energy absorption enhancement of pleated plate versus **a** a and **b** t_a

$$EAE_f = 0.157\left(\frac{\theta_o \pi}{180}\right)^{-1.158}\frac{\rho_f}{\sigma_p}V_m^2 + 0.0497\left(\frac{\theta_o \pi}{180}\right)^{8.373}\sqrt{\frac{\rho_f}{\sigma_p}}V_m + 1 \tag{3}$$

where ρ_f (kg/m^3) and σ_p (Pa) are density and plateau stress of aluminum foam, respectively, and V_m (m/s) is peak crushing velocity. As for the energy absorption enhancement of pleated plate, it was found to be strongly dependent on a, t_a, angle θ_o and t_p. Hence, an empirical equation in Eq. (4) was also derived in terms of four non-dimensional parameters to predict the energy absorption enhancement of pleated plate.

$$EAE_p = 0.0137\left(\frac{\rho_s a D}{\sigma_y}\right)^{1.483}\left(\frac{t_p}{D}\right)^{-1.247} \times \left(\frac{\theta_o \pi}{180}\right)^{-2.197}\left(\sqrt{\frac{a}{D}}t_a\right)^{2.236} + 1 \tag{4}$$

where ρ_s (kg/m^3) and σ_y (Pa) are density and yield strength of pleated plate, respectively, a (m/s^2) is positive acceleration, t_p (m) is pleated plate thickness, D (m) is aluminum foam depth and t_a (s) is positive acceleration duration. The empirical equations for predicting the energy absorption enhancements of aluminum foam and pleated plate are compared with numerical results in Figs. 23 and 24, respectively. It is noted that the empirical equations can provide close predictions as compared to the numerical results. With the empirical equations for predicting the energy absorption enhancements of aluminum foam and pleated plate as well as the analytical force–displacement function of the quasi-static loaded connector proposed by Wang et al. (2017a), the force–displacement function of the connector under dynamic crushing can be determined by scaling up the analytical force–displacement relation of the quasi-static loaded connector with the energy absorption enhancement for each component as follow:

$$F_D = EAE_p \cdot F_{pp} + EAE_f \cdot F_f \tag{5}$$

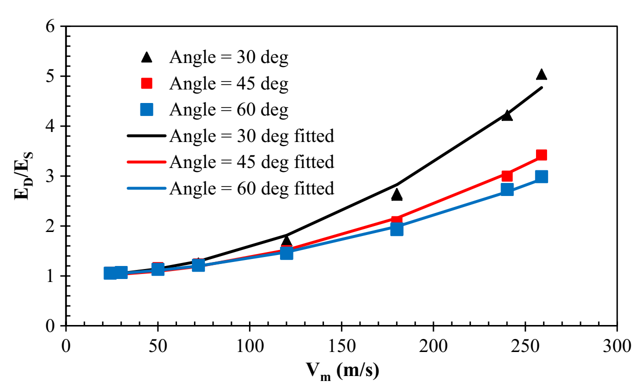

Fig. 23 Comparison of numerical results with the empirical equations for aluminum foam

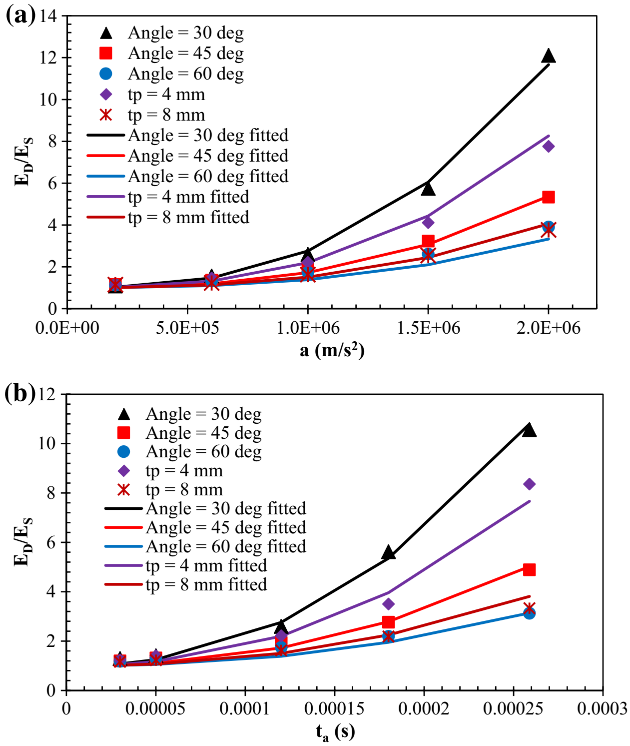

Fig. 24 Comparison of numerical results with the empirical equations for pleated plate: **a** varying with a and **b** varying with t_a

where F_D is crushing force of the dynamic loaded connector, F_{pp} and F_f are crushing forces contributed by aluminum foam and pleated plate, respectively, in the quasi-static crushing case (Wang et al. 2017). Hence, the analytical formula for predicting force–displacement relation of the dynamic loaded connector can be adopted for the blast resistant design.

5 Conclusions

In this paper, the dynamic crushing behaviors of the aluminum foam filled energy absorption connectors were numerically studied and the different deformation modes of the connector under quasi-static and dynamic crushing loads were also revealed. Then, the parametric studies on the effects of crushing velocity–time history, angle θ_o and pleated plate thickness on the energy absorption enhancement were conducted, based on which, two empirical equations were derived in terms of various parameters to predict the energy absorption enhancements of aluminum foam and pleated plate. The main findings from this work were summarized as follows:

(1) The deformation mode of the connector under dynamic crushing showed some differences as compared to that under quasi-static crushing, i.e., the crushing of aluminum foam initiated at the top and the upper pleated plate initially bended upward under dynamic crushing. The change of deformation mode under dynamic crushing could be attributed to the inertia force which changed the force distribution on the connector.
(2) The energy absorption of the connector showed significant increase under dynamic crushing as compared to that under quasi-static crushing and the pleated plate showed more evident energy absorption improvement as compared to aluminum foam. The improvement of energy absorption could be attributed to the change of deformation mode (for aluminum foam and pleated plate) and strain rate effect (for pleated plate).
(3) It was noted from the numerical results that the energy absorption enhancement of aluminum foam was only related to peak crushing velocity, V_m, while the energy absorption enhancement of pleated plate was related to positive acceleration, a, and positive acceleration duration, t_a.
(4) The energy absorption enhancement of aluminum foam showed increase with decreasing angle θ_o, but it was rarely affected by the variation of pleated plate thickness. In terms of the energy absorption enhancement of pleated plate, it could be increased by reducing either angle θ_o or pleated plate thickness. This was because smaller angle θ_o had longer upper pleated plate which could lead to higher energy absorption enhancement via plastic strain energy accumulation by the change of hogging moment to sagging moment during dynamic crushing. In addition, thinner pleated plate might behave more significant deformation mode change, which resulted in more significant increase of energy absorption.

Acknowledgements The research presented in this paper is financially supported by the National Natural Science Foundation of China (Grant No.: 51608151), the China Postdoctoral Science Foundation (Grant No.: 2016M600252 and 2017T100245) and Heilongjiang Postdoctoral Fund (Grant No.: LBH–Z16063).

References

Amadio, C., & Bedon, C. (2012a). Viscoelastic spider connectors for the mitigation of cable-supported facades subjected to air blast loading. *Engineering Structures, 42,* 190–200.
Amadio, C., & Bedon, C. (2012b). Elastoplastic dissipative devices for the mitigation of blast resisting cable-supported glazing façades. *Engineering Structures, 39,* 103–115.
Amadio, C., & Bedon, C. (2014). FE assessment of dissipative devices for the blast mitigation of glazing facades supported by prestressed cables. *Structural Engineering & Mechanics, 51*(1), 141–162.
Baroutaji, A., Gilchrist, M. D., & Olabi, A. G. (2016). Quasi-static, impact and energy absorption of internally nested tubes subjected to lateral loading. *Thin-Walled Structures, 98,* 337–350.

Baroutaji, A., Gilchrist, M. D., Smyth, D., & Olabi, A. G. (2015a). Crush analysis and multi-objective optimization design for circular tube under quasi-static lateral loading. *Thin-Walled Structures, 86,* 121–131.

Baroutaji, A., Gilchrist, M. D., Smyth, D., & Olabi, A. G. (2015b). Analysis and optimization of sandwich tubes energy absorbers under lateral loading. *International Journal of Impact Engineering, 82,* 74–88.

Baroutaji, A., Morris, E., & Olabi, A. G. (2014). Quasi-static response and multi-objective crashworthiness optimization of oblong tube under lateral loading. *Thin-Walled Structures, 82,* 262–277.

Chen, X., Gao, G., Dong, H., & Li, J. (2016). Experimental and numerical investigations of a splitting-bending steel plate energy absorber. *Thin-Walled Structures, 98,* 384–391.

Fan, H., Hong, W., Sun, F., Xu, Y., & Jin, F. (2015). Lateral compression behaviors of thin-walled equilateral triangular tubes. *International Journal of Steel Structures, 15*(4), 785–795.

Fan, Z., Shen, J., Lu, G., & Ruan, D. (2013). Dynamic lateral crushing of empty and sandwich tubes. *International Journal of Impact Engineering, 53,* 3–16.

Gupta, N. K., Sekhon, G. S., & Gupta, P. K. (2005). Study of lateral compression of round metallic tubes. *Thin-Walled Structures, 43,* 895–992.

Hall, I. W., Guden, M., & Claar, T. D. (2002). Transverse and longitudinal crushing of aluminum-foam filled tubes. *Scripta Materialia, 46,* 513–518.

Hallissy G, Higbie WG, Fyfe ER. Blast resistant prefabricated wall units. US Patent, Pub. No.: US2005/0144900 A1, 2005.

Hallquist, J. O. (2006). *LS-DYNA theory manual, Livermore Software Technology Corporation (LSTC)*. California, USA: Livermore.

Hallquist, J. O. (2012). *LS-DYNA keyword user's manual, Livermore Software Technology Corporation (LSTC)*. California, USA: Livermore.

Hanssen, A. G., Hopperstad, O. S., Langseth, M., & Ilstand, H. (2002). Validation of constitutive models applicable to aluminium foams. *International Journal of Mechanical Sciences, 44,* 359–406.

Huang, Z., & Liew, J. Y. R. (2016). Compressive resistance of steel-concrete-steel sandwich composite walls with J-hook connectors. *Journal of Constructional Steel Research, 124,* 142–162.

Huang, Z., Liew, J. Y. R., Xiong, M., & Wang, J. (2015). Structural behaviour of double skin composite system using ultra-lightweight cement composite. *Construction and Building Materials, 86,* 51–63.

Jones, N. (1988). *Structural impact*. Cambridge/New York: Cambridge University Press.

McDevitt, T. J., & Simmonds, J. G. (2003). Crushing of an elastic-plastic ring between rigid plates with and without unloading. *Journal of Applied Mechanics, 70,* 799–808.

Ngo, T., Ding, C., Lumantarna, R., Ghazlan, A., & Zobec, M. (2015). Structural performance of double-skin façade systems subjected to blast pressures. *Journal of Structural Engineering, 141*(12), 04015064.

Niknejad, A., & Orojloo, P. H. (2016). A novel nested system of tubes with special cross-section as the energy absorber. *Thin-Walled Structures, 100,* 113–123.

Olabi, A. G., Morris, E., Hashmi, M. S. J., & Gilchrist, M. D. (2008a). Optimised design of nested circular tube energy absorbers under lateral impact loading. *International Journal of Mechanical Sciences, 50,* 104–116.

Olabi, A. G., Morris, E., Hashmi, M. S. J., & Gilchrist, M. D. (2008b). Optimised design of nested oblong tube energy absorbers under lateral impact loading. *International Journal of Impact Engineering, 35,* 10–26.

Qi, C., Yang, S., Yang, L. J., Wei, Z. Y., & Lu, Z. H. (2013). Blast resistance and multi-objective optimization of aluminum foam-cored sandwich panels. *Composite Structures, 105,* 45–57.

Reyes, A., Hopperstad, O. S., Berstad, T., Hanssen, A. G., & Langseth, M. (2003). Constitutive modeling of aluminum foam including fracture and statistical variation of density. *European Journal of Mechanics A/Solids, 22,* 815–835.

Reyes, A., Hopperstad, O. S., Hanssen, A. G., & Langseth, M. (2004a). Modeling of material failure in foam-based components. *International Journal of Impact Engineering, 30,* 805–834.

Reyes, A., Hopperstad, O. S., & Langseth, M. (2004b). Aluminum foam-filled extrusions subjected to oblique loading: Experimental and numerical study. *International Journal of Solids and Structures, 41,* 1645–1675.

Santosa, S. P., Wierzbicki, T., Hanssen, A. G., & Langseth, M. (2000). Experimental and numerical studies of foam-filled sections. *International Journal of Impact Engineering, 24,* 509–534.

Shahbeyk, S., Petrinic, N., & Vafai, A. (2007). Numerical modelling of dynamically loaded metal foam-filled square columns. *International Journal of Impact Engineering, 34,* 573–586.

Shen, J., Lu, G., Ruan, D., & Seah, C. C. (2015). Lateral plastic collapse of sandwich tubes with metal foam core. *International Journal of Mechanical Sciences, 91,* 99–109.

Shim, C. S., Yun, N. R., Shin, D. H., & Yu, I. H. (2013). Design of protective structures with aluminum foam panels. *International Journal of Steel Structures, 13*(1), 1–10.

Smith, R., Altenhof, W., & Lapain, M. (2016). Transverse impact loading of aluminum foam filled braided stainless steel tubes. *International Journal of Impact Engineering, 88,* 214–226.

Su, X. Y., Yu, T. X., & Reid, S. R. (1995a). Inertia-sensitive impact energy-absorbing structures part I: Effects of inertia and elasticity. *International Journal of Impact Engineering, 16*(4), 651–672.

Su, X. Y., Yu, T. X., & Reid, S. R. (1995b). Inertia-sensitive impact energy-absorbing structures part II: Effects of strain rate. *International Journal of Impact Engineering, 6*(4), 673–689.

Wang, C. Y. (1987). Crushing of an elastic-perfectly plastic ring or tube between two planes. *Journal of Applied Mechanics, 54,* 159–164.

Wang, Y., & Liew, J. Y. R. (2015). Blast performance of water tank with energy absorbing support. *Thin-Walled Structures, 96,* 1–10.

Wang, Y., Liew, J. Y. R., & Lee, S. C. (2015). Structural performance of water tank under static and dynamic pressure loading. *International Journal of Impact Engineering, 85,* 110–123.

Wang, Y., Liew, J. Y. R., & Lee, S. C. (2016). A novel multi-functional water façade system for energy saving and blast resisting. *Materials and Design, 106,* 98–111.

Wang, Y., Liew, J. Y. R., Lee, S. C., & Wang, W. (2017a). Experimental and analytical studies of a novel aluminum foam filled energy absorption connector under quasi-static compression loading. *Engineering Structures, 131,* 136–147.

Wang, Y., Liew, J. Y. R., Lee, S. C., Zhai, X., & Wang, W. (2017b). Crushing of a novel energy absorption connector with curved plate and aluminum foam as energy absorber. *Thin-Walled Structures, 111,* 145–154.

Wang, Y., Zhai, X., & Wang, W. (2017c). Numerical studies of aluminum foam filled energy absorption connectors under quasi-static compression loading. *Thin-Walled Structures, 116,* 225–233.

Whitney, M. G. (1996). *Blast damage mitigation using reinforced concrete panels and energy absorbing connectors*. San Antonio, TX: Wilfred Baker Engineering Inc.

Yang, S., & Qi, C. (2013). Multiobjective optimization for empty and foam-filled square columns under oblique impact loading. *International Journal of Impact Engineering, 54,* 177–191.

Zhang, X., Cheng, G., & Zhang, H. (2009). Numerical investigations on a new type of energy-absorbing structure based on free inversion of tubes. *International Journal of Mechanical Sciences, 51,* 64–76.

Zhang, X., Hao, H., & Wang, Z. (2015). Experimental study of laminated glass window responses under impulsive and blast loading. *International Journal of Impact Engineering, 78,* 1–19.

Zhu, H., & Khanna, S. K. (2016). Dynamic response of a novel laminated glass panel using a transparent glass fiber-reinforced composite interlayer under blast loading. *International Journal of Impact Engineering, 89,* 14–24.